Supporting Information

Visualizing Temperature Inhomogeneity Using Thermo-Responsive Smart Materials

Panqin Wang [a], Jiaren Du [a], Tengyue Wang [a], Shaoxing Lyu [a], Rik Van Deun [b], Dirk Poelman [c,d] and Hengwei Lin [a]**

AUTHOR ADDRESS

[a] International Joint Research Center for Photo-responsive Molecules and Materials, School of Chemical and Material Engineering, Jiangnan University, 214122, Wuxi, China;

[b] L^3–Luminescent Lanthanide Lab, Department of Chemistry, Ghent University, Krijgslaan 281-S3, B-9000 Ghent, Belgium.

[c] LumiLab, Department of Solid State Sciences, Ghent University, Krijgslaan 281-S1, B-9000, Ghent, Belgium.

[d] Center for Nano- and Biophotonics (NB-Photonics), Ghent University, B-9000, Ghent, Belgium.

AUTHOR INFORMATION

***Corresponding authors:**

Dr. Jiaren Du (jiaren.du@jiangnan.edu.cn)

Prof. Hengwei Lin (linhengwei@jiangnan.edu.cn)

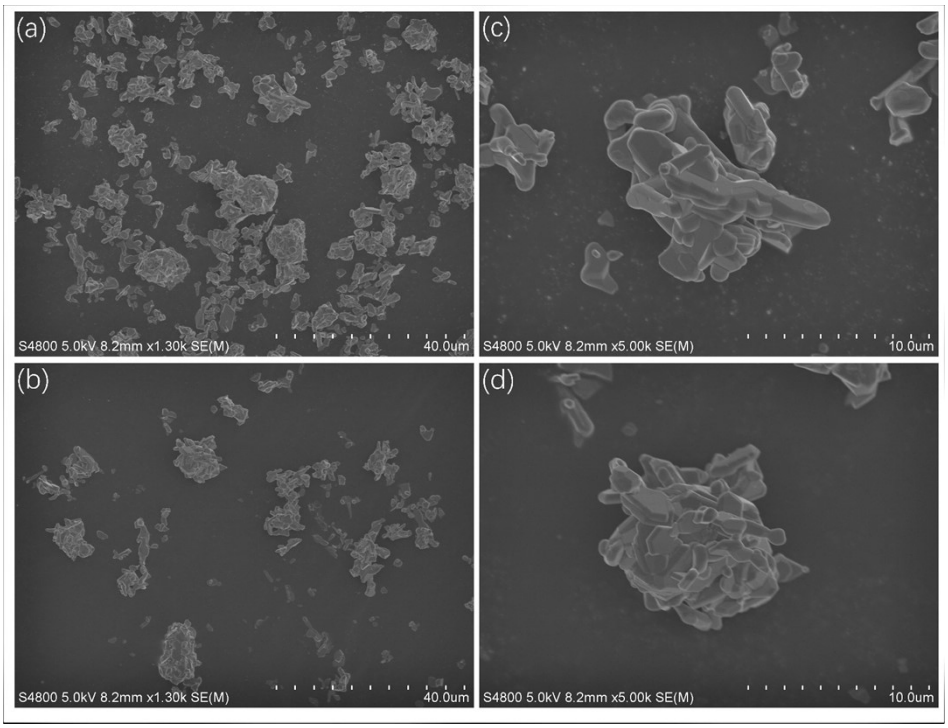

Figure S1. SEM morphology of $SrGa_{12-x}Al_xO_{19}$:4%Dy^{3+} (x=3) phosphor of the selected area with varied scales (a)-(b) 40 μm, and (c)-(d) 10 μm, respectively.

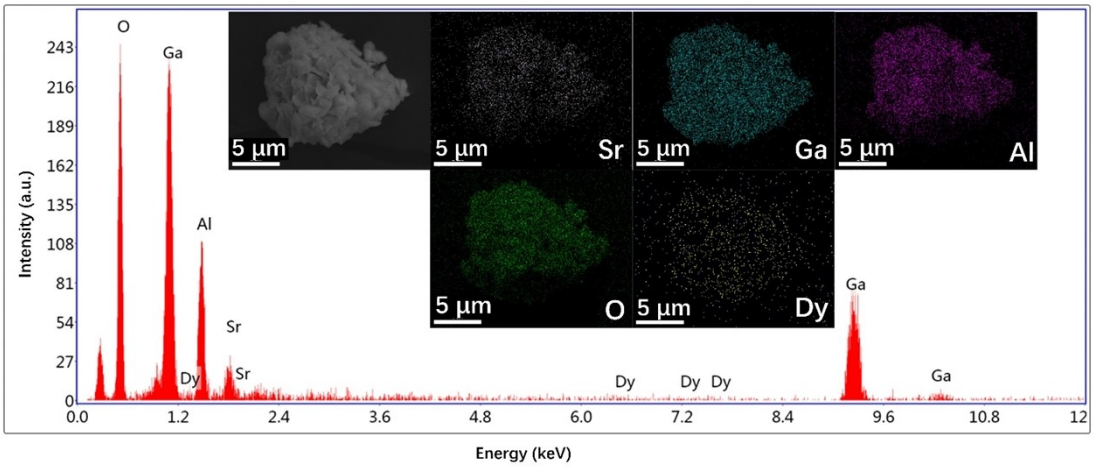

Figure S2. EDS elemental mappings of $SrGa_{12-x}Al_xO_{19}$:4%Dy^{3+} (x=3) phosphor. Elemental mapping images of Sr, Ga, Al, O and Dy for the selected microparticle.

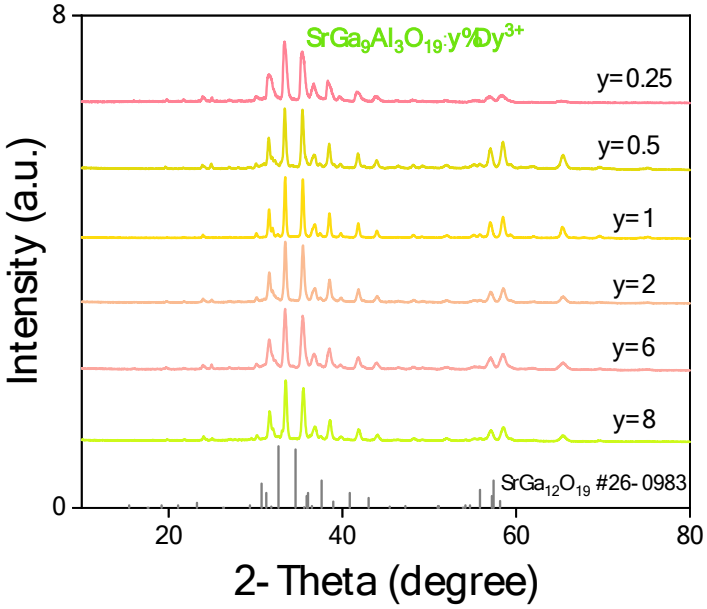

Figure S3. XRD patterns of $SrGa_9Al_3O_{19}$:y%Dy^{3+} samples. Dy^{3+} concentration is 0.25%, 0.5%, 1%, 2%, 6%, 8%, respectively.

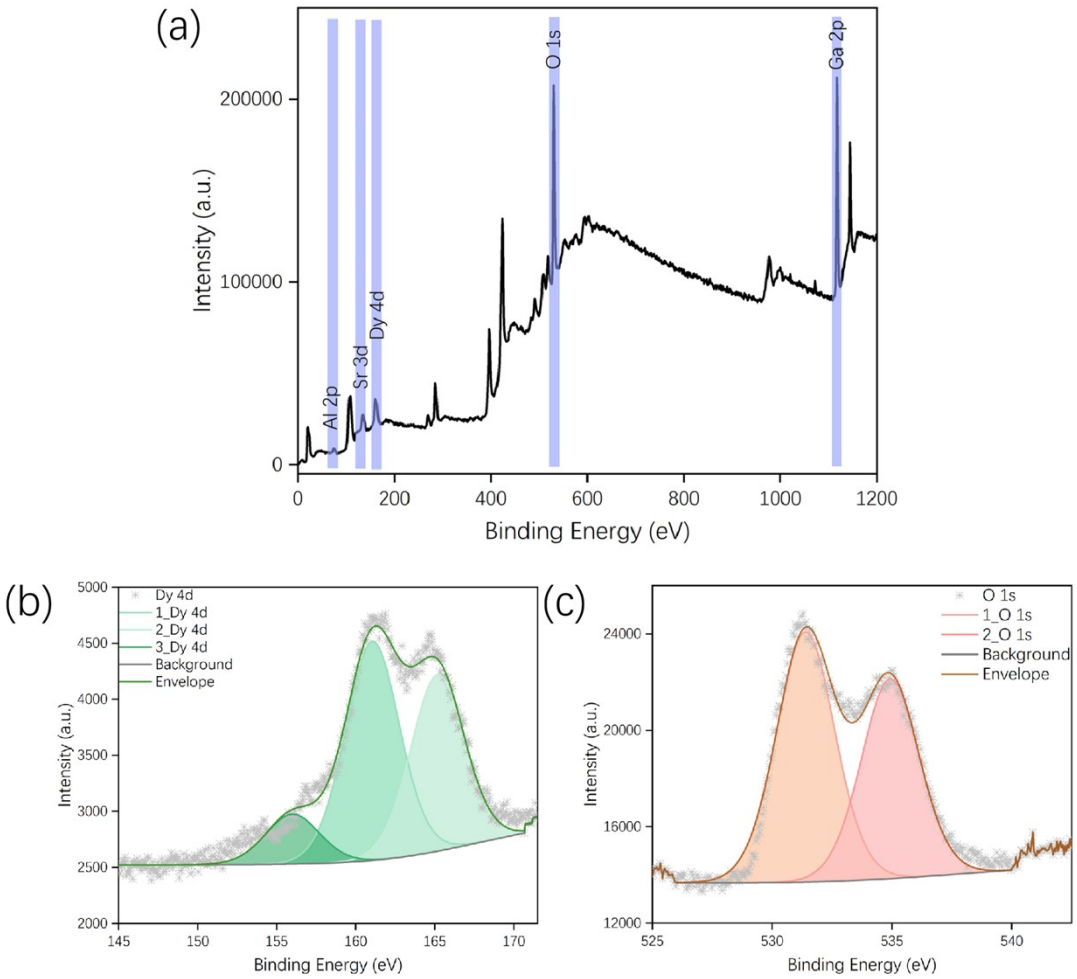

Figure S4. XPS survey of $SrGa_{12-x}Al_xO_{19}$:4%Dy^{3+} (x=3). (a) The whole spectrum of $SrGa_{12-x}Al_xO_{19}$:4%Dy^{3+} (x=3). Magnified XPS peaks with fitting curves for Dy (b) and O (c) from the $SrGa_{12-x}Al_xO_{19}$:4%Dy^{3+} (x=3) phosphor.

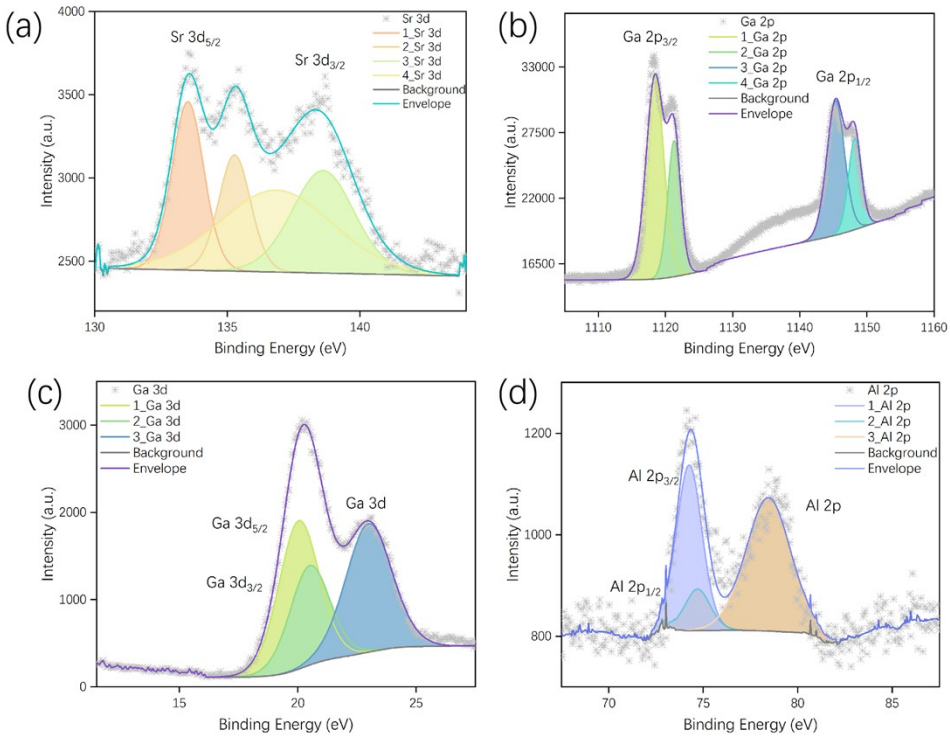

Figure S5. Magnified XPS peaks with fitting curves for Sr 3d (a), Ga 2p (b), Ga 3d (c), Al 2p (d) in $SrGa_{12-x}Al_xO_{19}$:4%Dy^{3+} (x=3) phosphor.

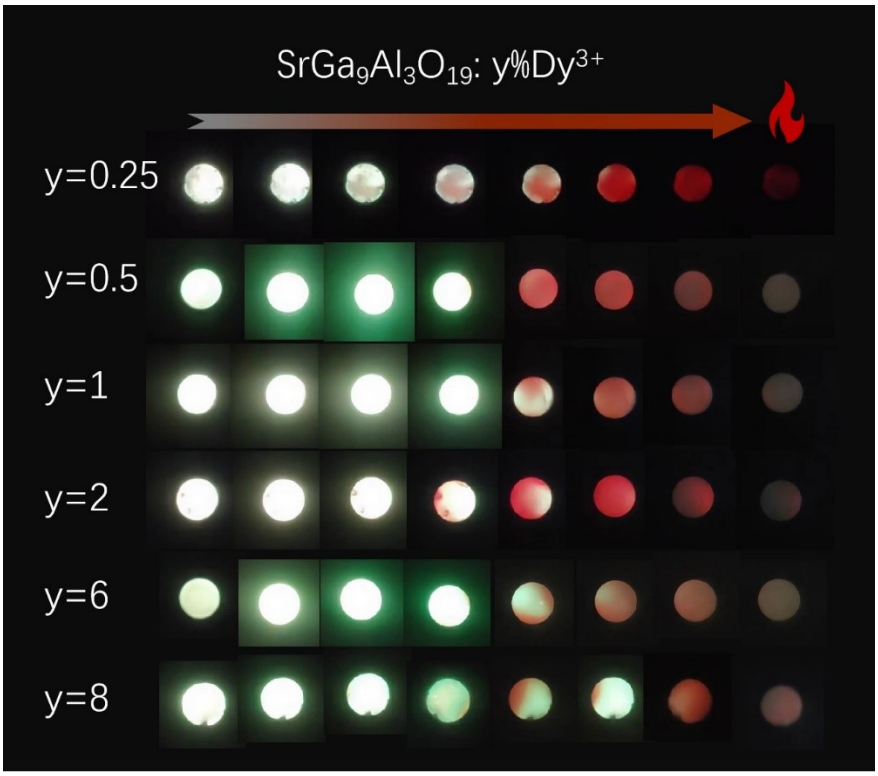

Figure S6. Photographs of thermally stimulated luminescence of $SrGa_9Al_3O_{19}$:y%Dy^{3+} (y = 0.25%, 0.5%, 1%, 2%, 6%, 8%) after 254 nm pre-irradiation at room temperature.

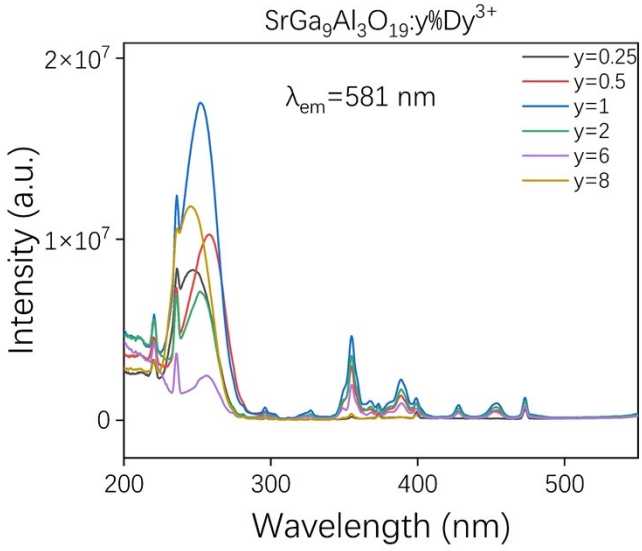

Figure S7. PLE spectra of $SrGa_9Al_3O_{19}$:y%Dy^{3+} samples. PLE spectra were monitored at emission of 581 nm.

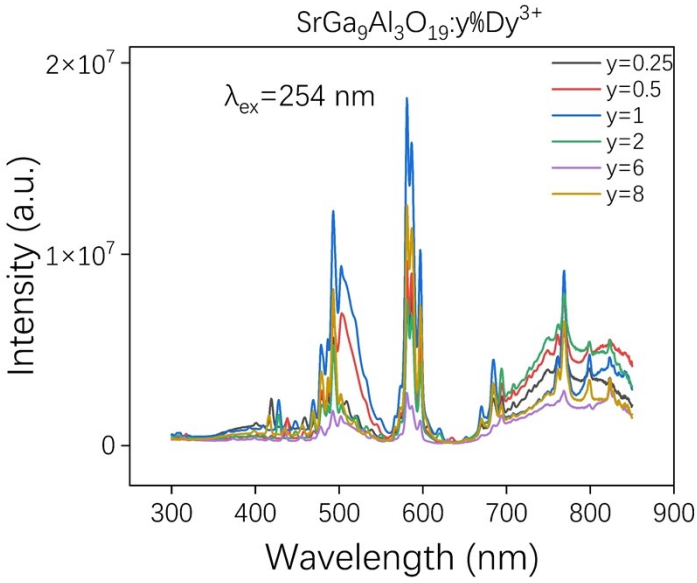

Figure S8. PL spectra of $SrGa_9Al_3O_{19}$:y%Dy^{3+} samples. PL spectra were collected upon 254 nm excitation.

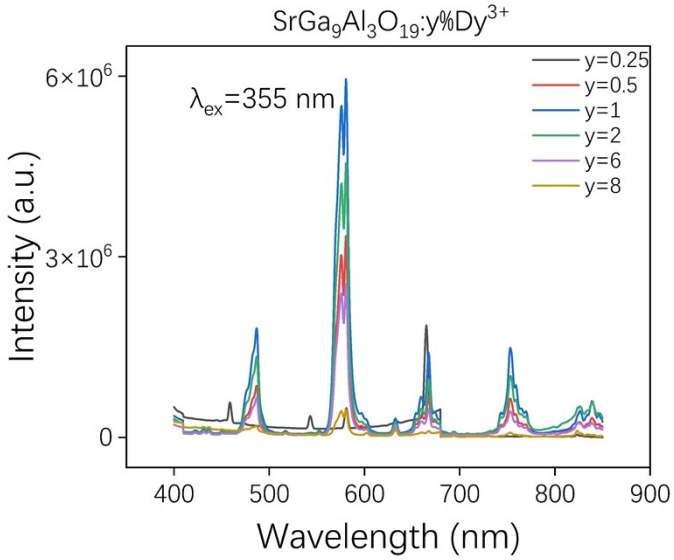

Figure S9. PL spectra of $SrGa_9Al_3O_{19}$:y%Dy^{3+} samples. PL spectra were collected upon 355 nm excitation.

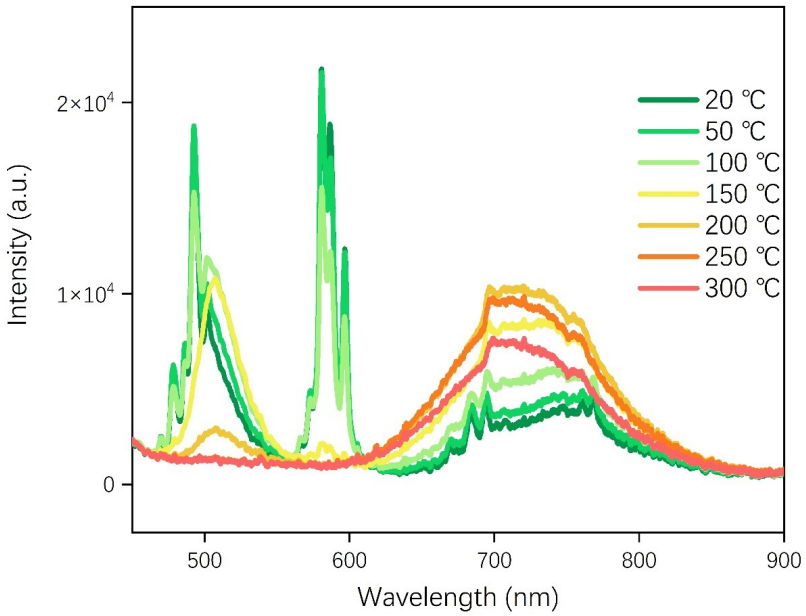

Figure S10. Temperature dependent emission from $SrGa_{12-x}Al_xO_{19}$:4%Dy^{3+} (x=2) phosphor upon 254 nm excitation. The ambient temperature was varied from 20 °C to 300 °C.

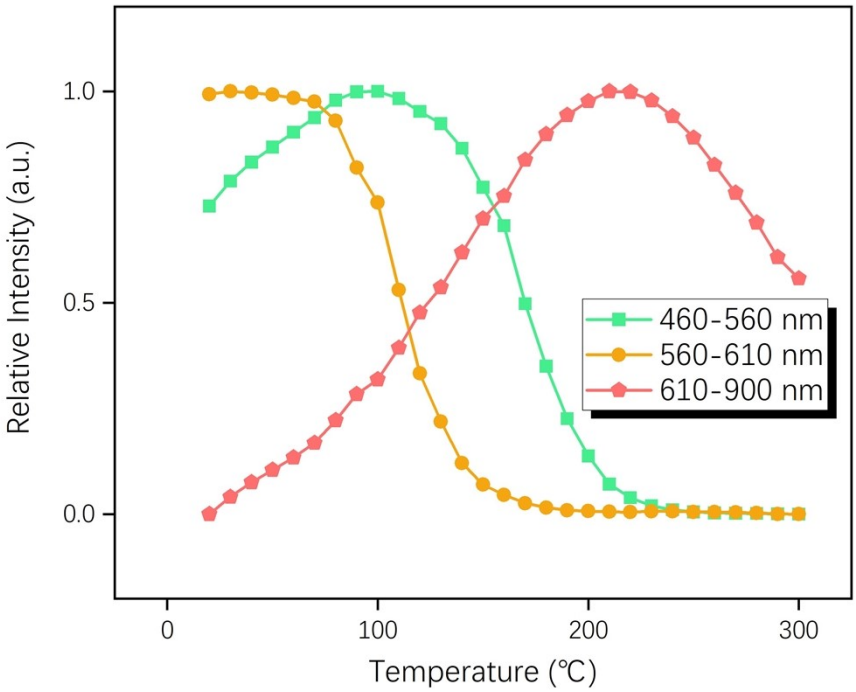

Figure S11. Integrated intensity of emissions in three wavelength regions of $SrGa_{12-x}Al_xO_{19}$:4%Dy^{3+} (x=2) phosphor. The ambient temperature was varied from 20 °C to 300 °C, and the wavelength region was divided into 460-560 nm, 560-610 nm, and 610-900 nm, respectively.

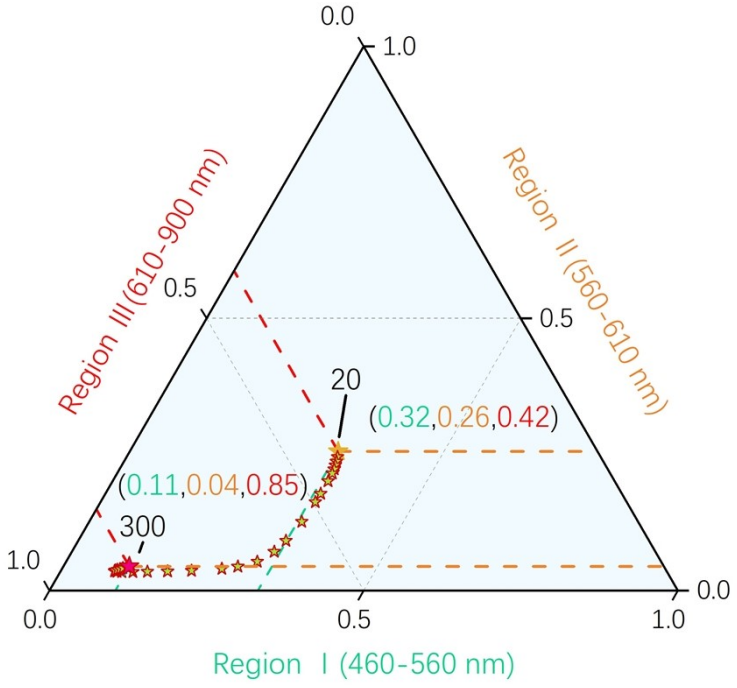

Figure S12. Relative proportion among three wavelength regions of $SrGa_{12-x}Al_xO_{19}$:4%Dy^{3+} (x=2) phosphor at varied temperatures.

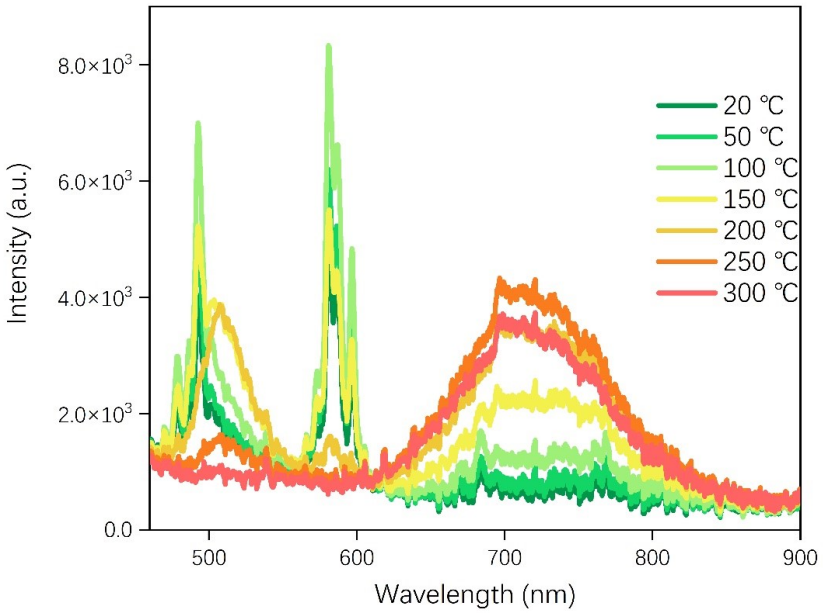

Figure S13. Temperature dependent emission from $SrGa_{12-x}Al_xO_{19}$:4%Dy^{3+} (x=3) phosphor upon 254 nm excitation. The ambient temperature was varied from 20 °C to 300 °C.

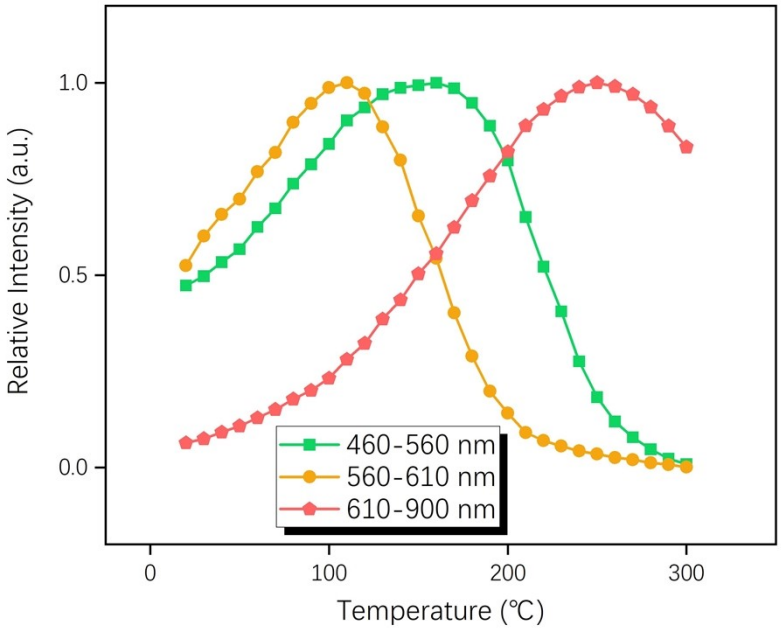

Figure S14. Integrated intensity of emissions in three wavelength regions of $SrGa_{12-x}Al_xO_{19}$:4%Dy^{3+} (x=3) phosphor. The ambient temperature was varied from 20 °C to 300 °C, and the wavelength region was divided into 460-560 nm, 560-610 nm, and 610-900 nm, respectively.

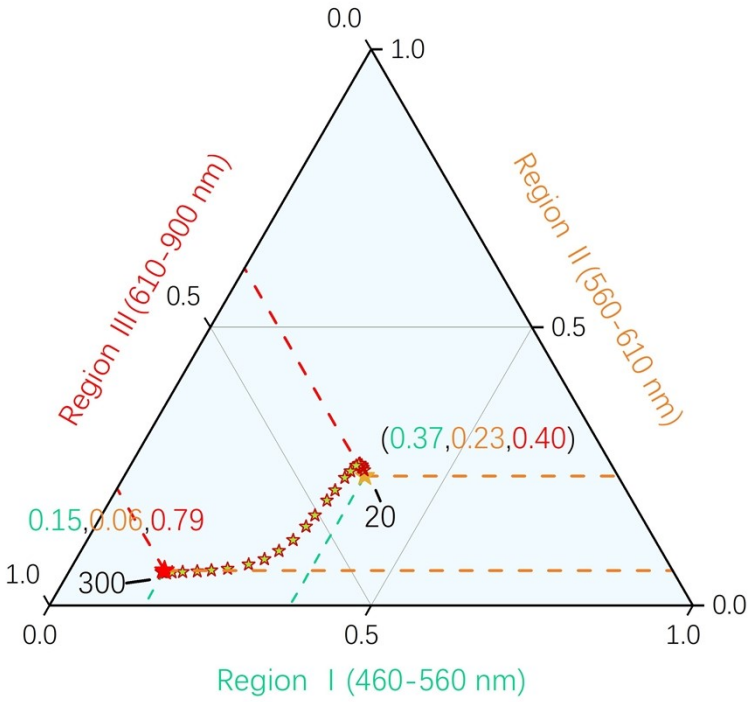

Figure S15. Relative proportion among three wavelength regions of $SrGa_{12-x}Al_xO_{19}$:4%Dy^{3+} (x=3) phosphor at varied temperatures.

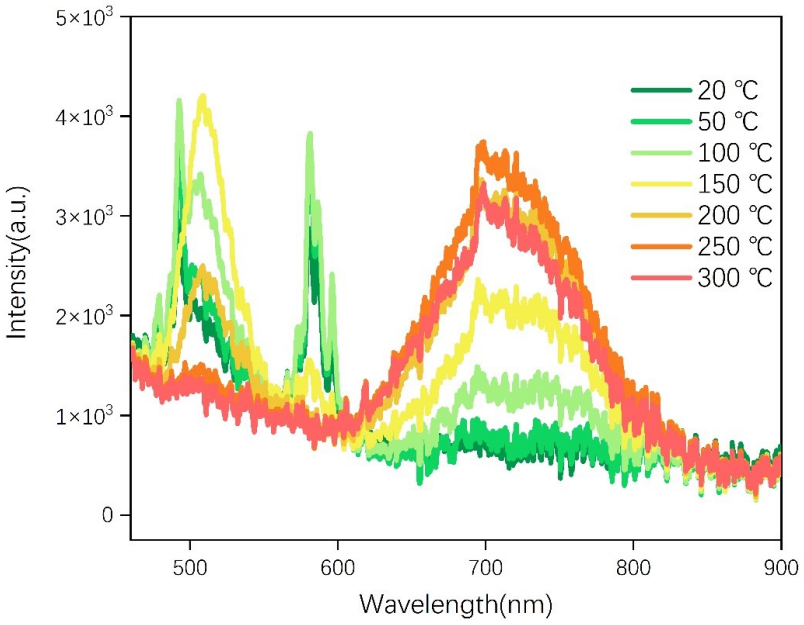

Figure S16. Temperature dependent emission from $SrGa_{12-x}Al_xO_{19}$:4%Dy^{3+} (x=4) phosphor upon 254 nm excitation. The ambient temperature was varied from 20 °C to 300 °C.

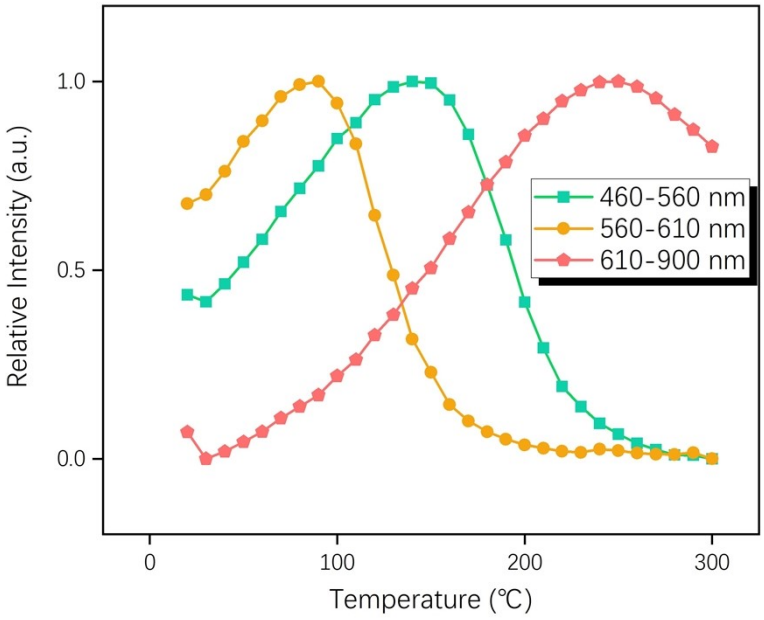

Figure S17. Integrated intensity of emissions in three wavelength regions of $SrGa_{12-x}Al_xO_{19}$:4%Dy^{3+} (x=4) phosphor. The ambient temperature was varied from 20 °C to 300 °C, and the wavelength region was divided into 460-560 nm, 560-610 nm, and 610-900 nm, respectively.

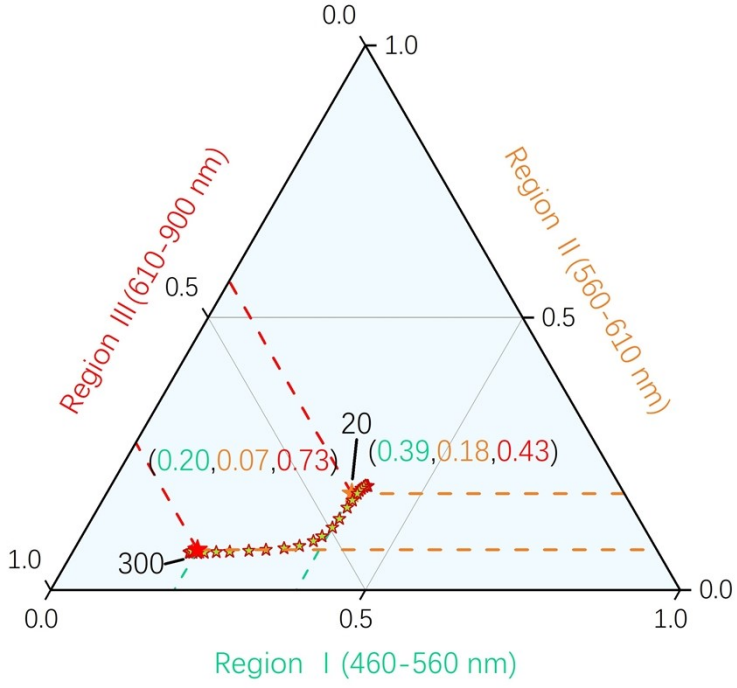

Figure S18. Relative proportion among three wavelength regions of $SrGa_{12-x}Al_xO_{19}$:4%Dy^{3+} (x=4) phosphor at varied temperatures.

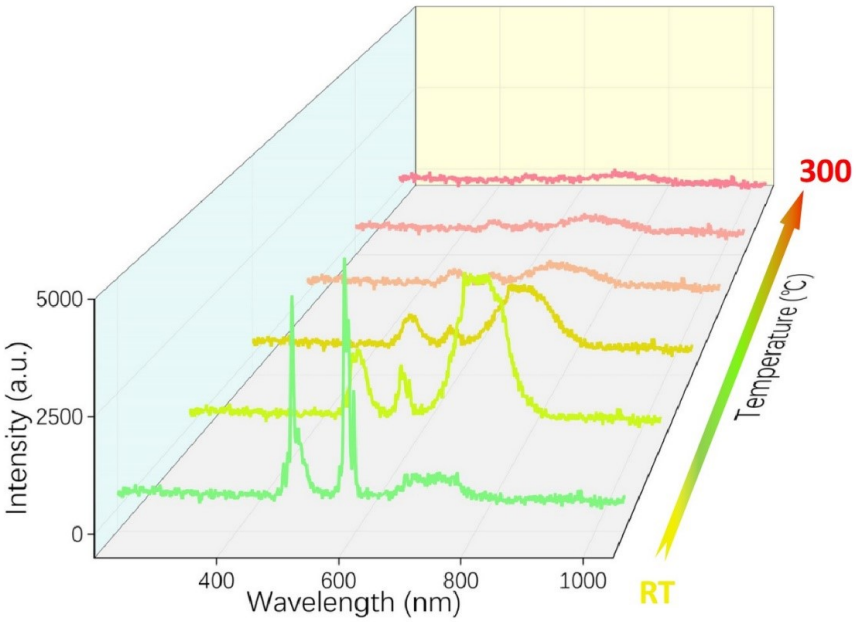

Figure S19. Thermally stimulated luminescence spectra of $SrGa_{12-x}Al_xO_{19}$:4%Dy^{3+} (x=2) after 254 nm irradiation.

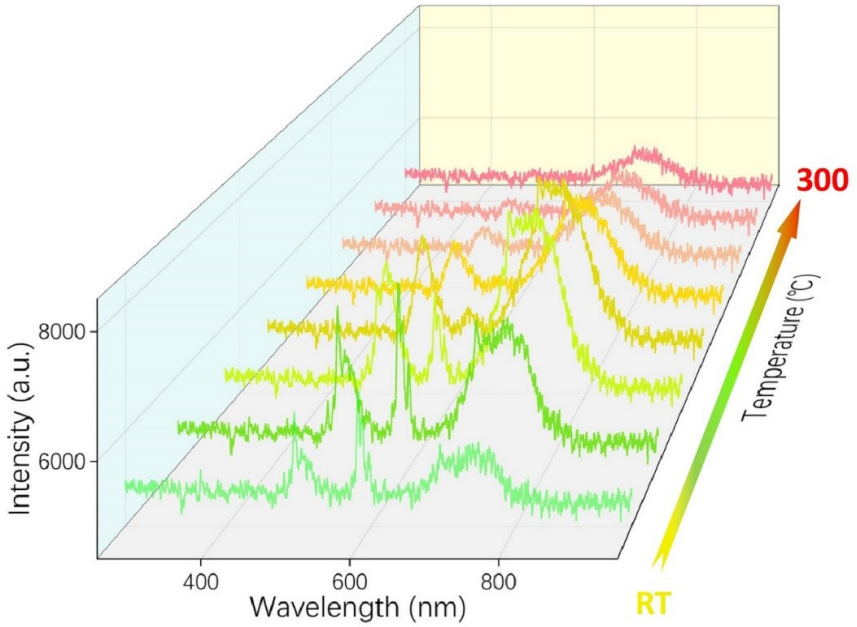

Figure S20. Thermally stimulated luminescence spectra of $SrGa_{12-x}Al_xO_{19}$:4%Dy^{3+} (x=3) after 254 nm irradiation.

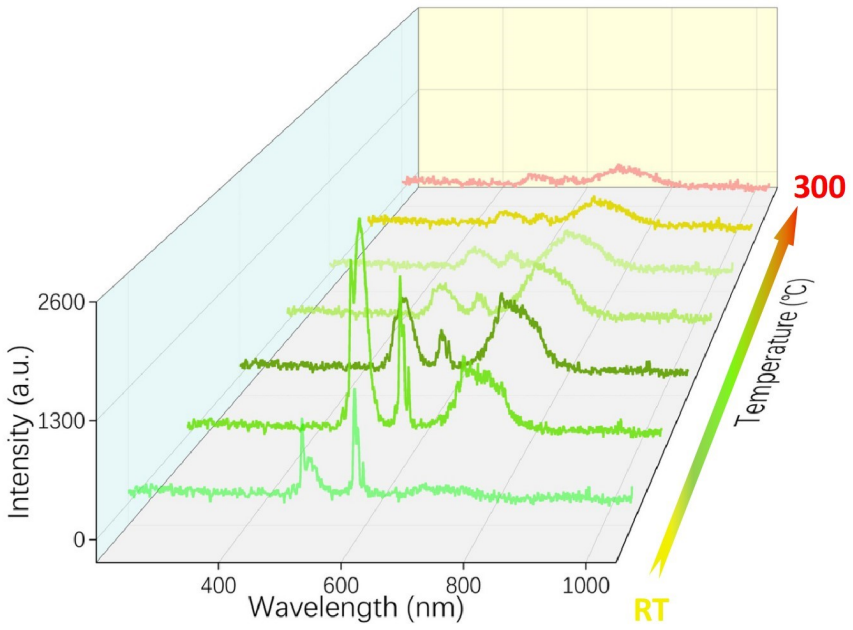

Figure S21. Thermally stimulated luminescence spectra of $SrGa_{12-x}Al_xO_{19}$:4%Dy^{3+} (x=4) after 254 nm irradiation.

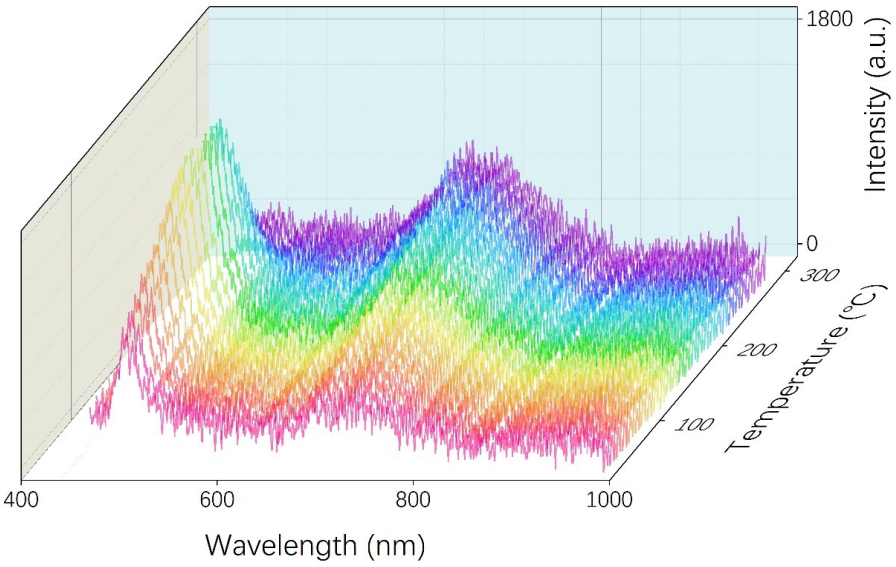

Figure S22. PL spectra of $SrGa_{12-x}Al_xO_{19}$ (x=2) at different temperatures under 254 nm excitation.

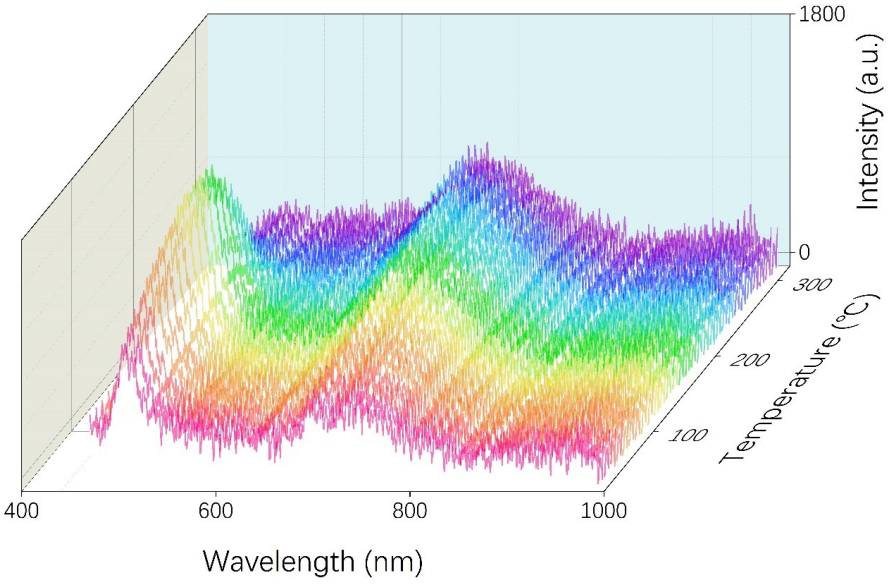

Figure S23. PL spectra of $SrGa_{12-x}Al_xO_{19}$ (x=3) at different temperatures under 254 nm excitation.

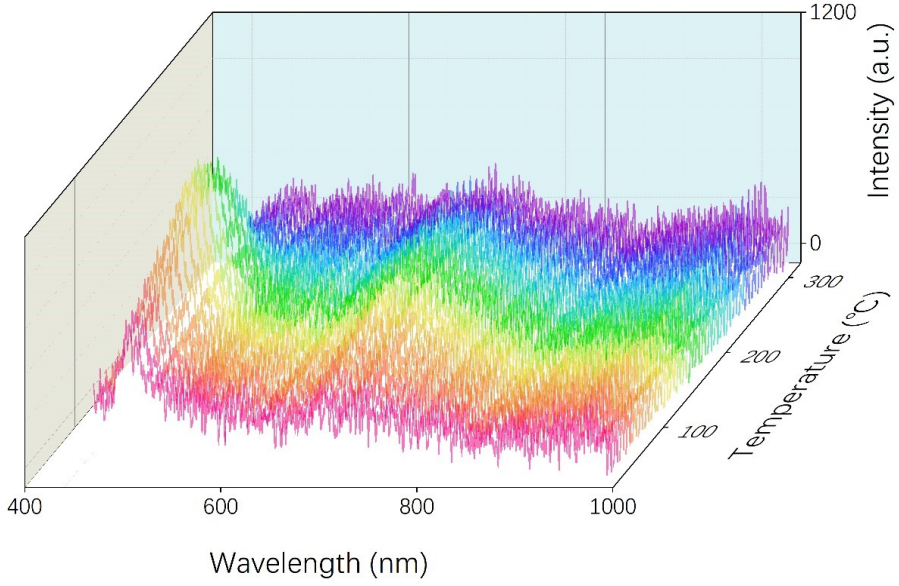

Figure S24. PL spectra of $SrGa_{12-x}Al_xO_{19}$ (x=4) at different temperatures under 254 nm excitation.

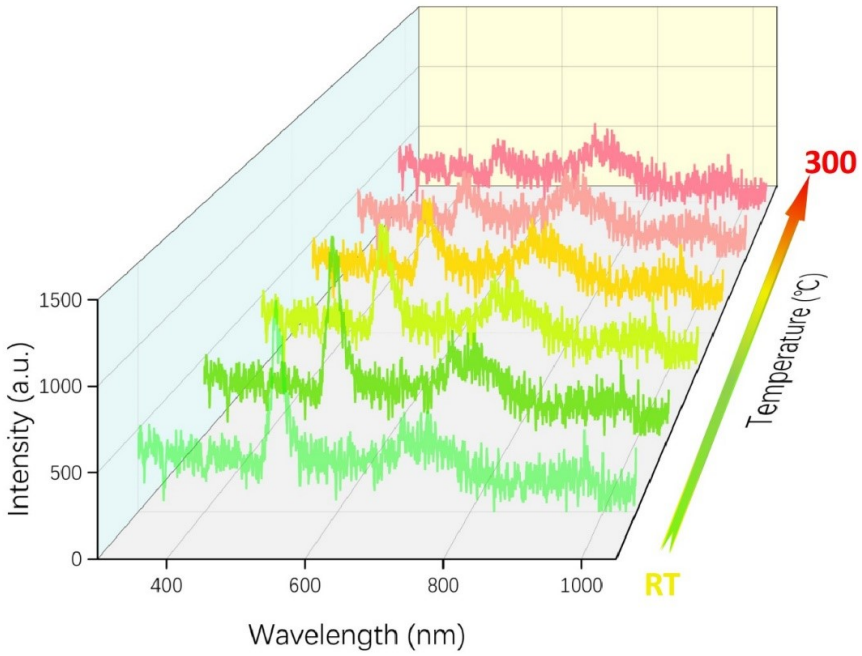

Figure S25. Thermally stimulated luminescence spectra of $SrGa_{12-x}Al_xO_{19}$ (x=3) after 254 nm irradiation.

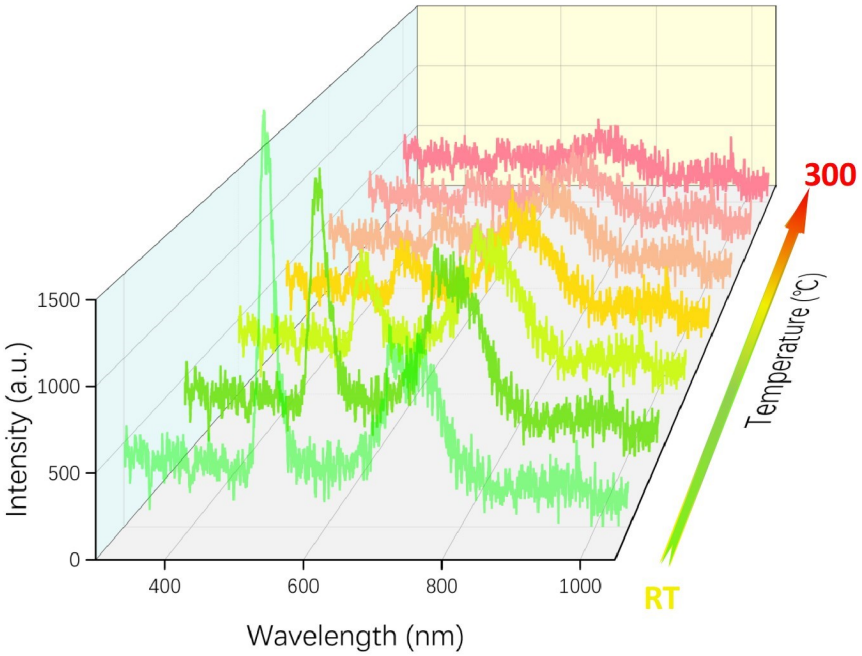

Figure S26. Thermally stimulated luminescence spectra of $SrGa_{12-x}Al_xO_{19}$ (x=4) after 254 nm irradiation.

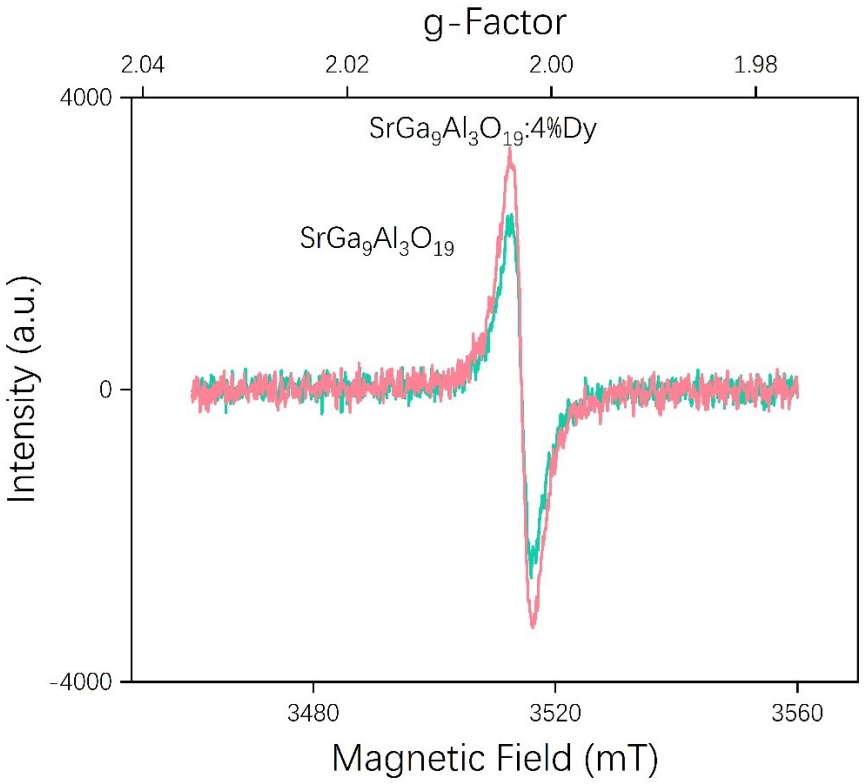

Figure S27. EPR spectra of $SrGa_{12-x}Al_xO_{19}$ (x=3, green curve) and $SrGa_{12-x}Al_xO_{19}$: 4%Dy^{3+} (x=3, red curve).

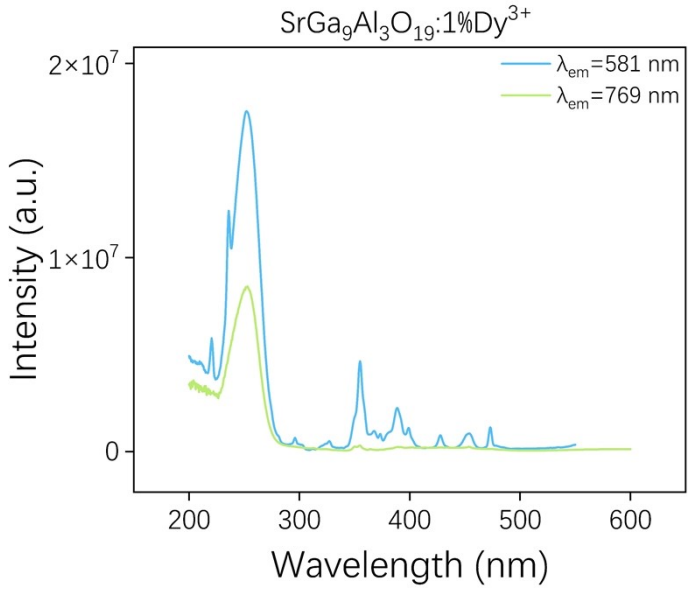

Figure S28. The comparison of excitation spectrum of the different emission features (λ_{em}=769 nm for the host emission and λ_{em}=581 nm for Dy^{3+} emission).

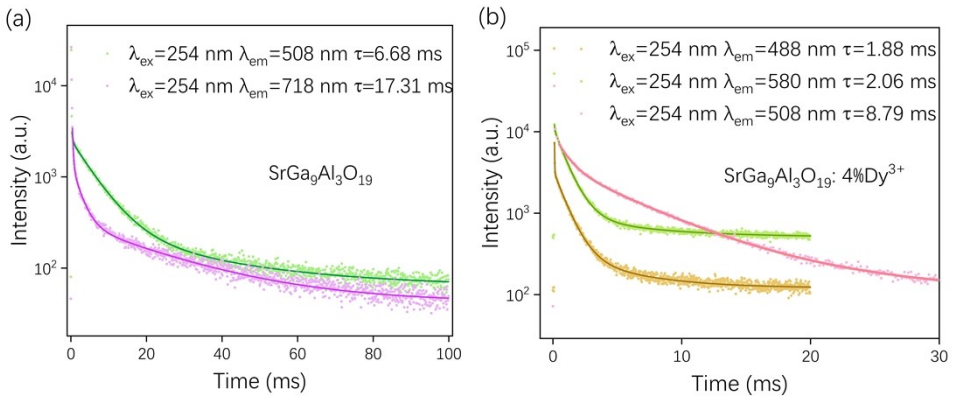

Figure S29. Luminescence decay curves of $SrGa_{12-x}Al_xO_{19}$ (x=3) and $SrGa_{12-x}Al_xO_{19}$: $4\%Dy^{3+}$ (x=3) upon the 254 nm excitation.

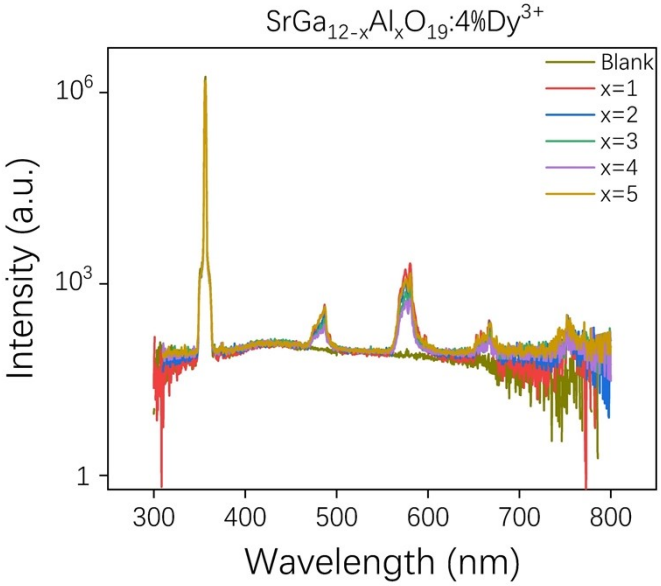

Figure S30. The photoluminescence quantum yield (PLQY) of $SrGa_{12-x}Al_xO_{19}:Dy^{3+}$ phosphors (x=1, 2, 3, 4, 5)

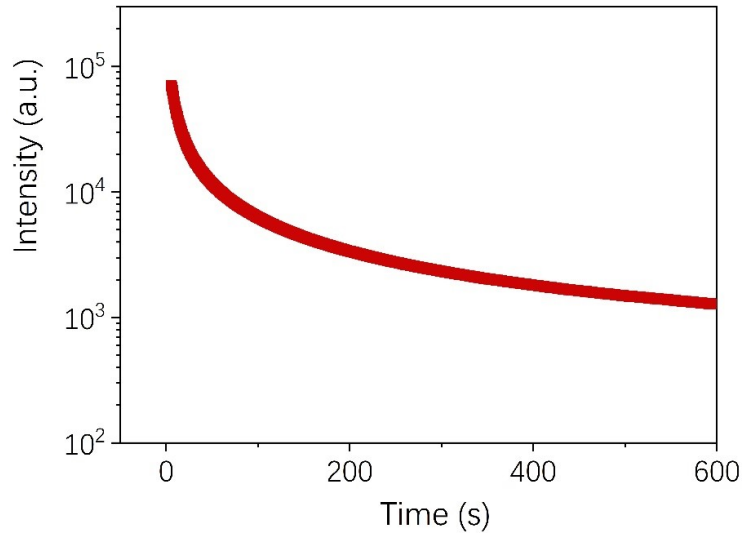

Figure S31. Persistent luminescence decay curve of $SrGa_{12-x}Al_xO_{19}$: 4%Dy^{3+} (x=3) after 254 nm excitation.

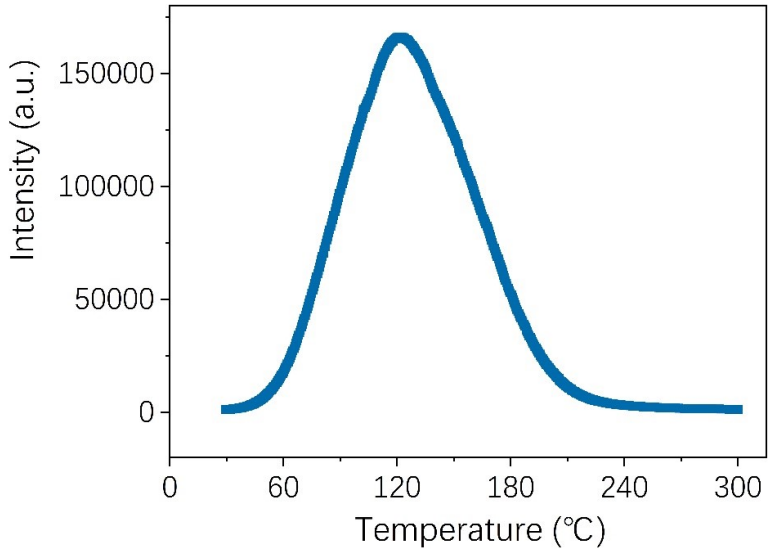

Figure S32. TL glow curves of $SrGa_{12-x}Al_xO_{19}$: 4%Dy^{3+} (x=3) after 254 nm excitation.

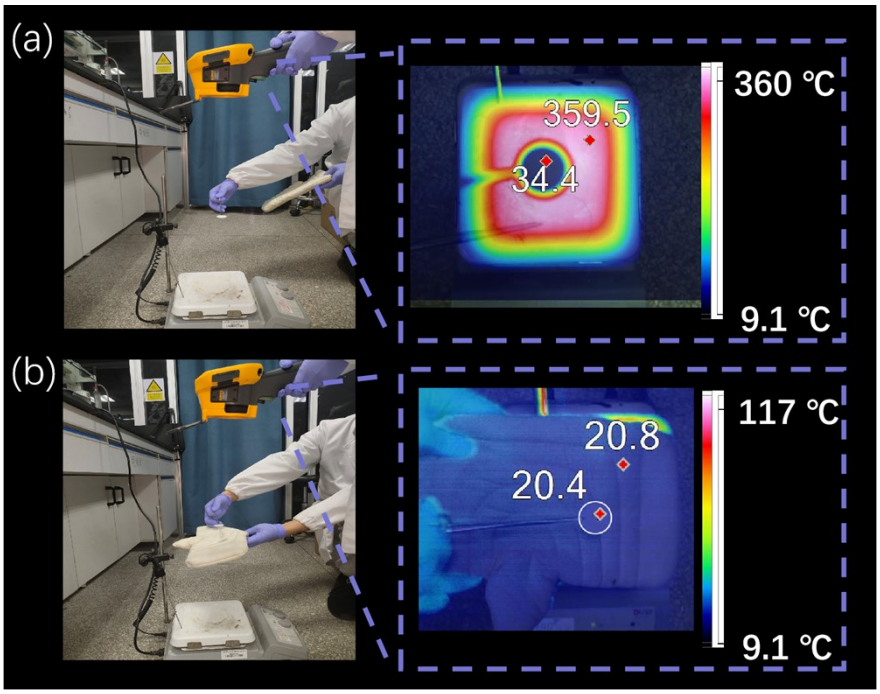

Figure S33. Demonstration of the measured distribution of thermal fields via infrared thermal imager at a high-temperature background (360 °C) or a shielded room-temperature background.

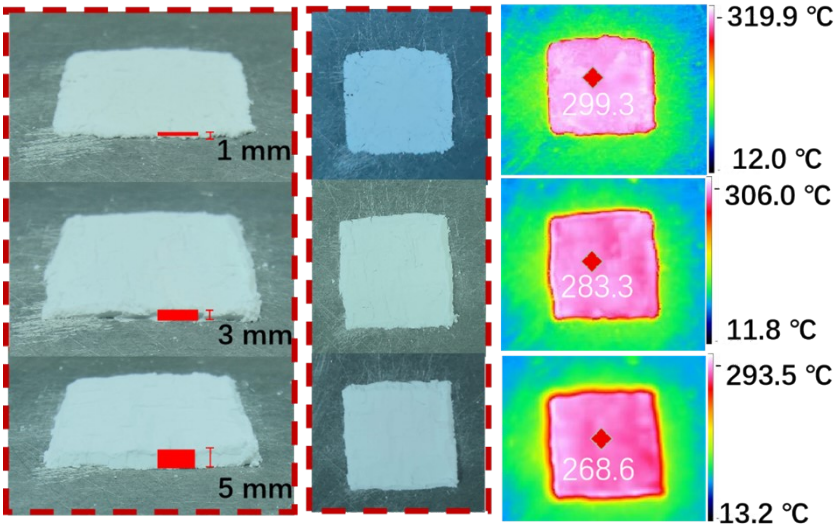

Figure S34. Temperature sensitivity of the $SrGa_{12-x}Al_xO_{19}$: 4%Dy^{3+} (x=3) phosphor. Thickness of the phosphor film was made at around 1 mm, 2 mm, and 5 mm, respectively. Demonstration of the measured distribution of thermal fields was performed via infrared thermal imager at ambient backgrounds (300 °C).

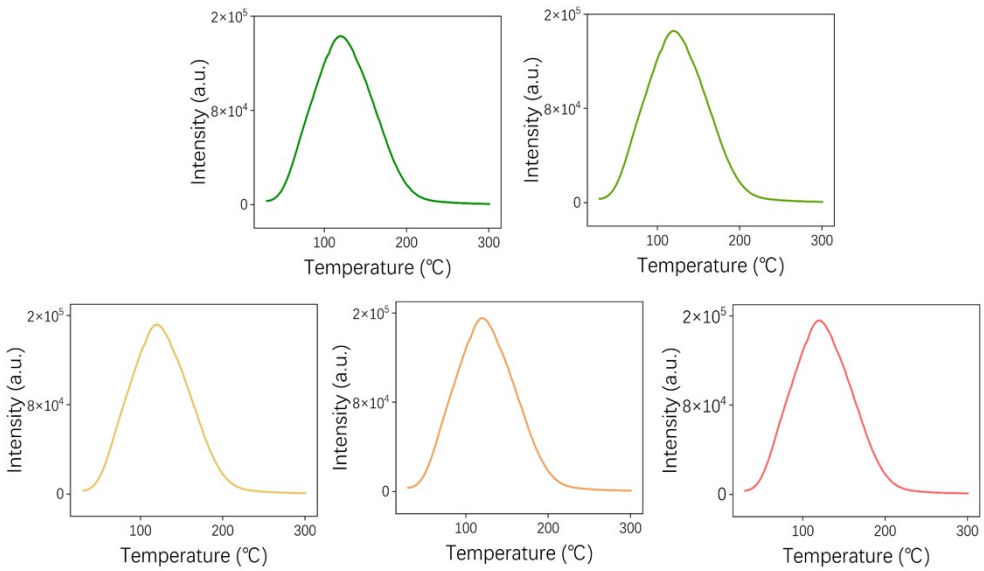

Figure S35. Thermal repeatability of the $SrGa_{12-x}Al_xO_{19}$: 4%Dy^{3+} (x=3) phosphor. TL-based temperature sensor was repeatedly checked via five cycle TL measurements. Phosphor was irradiated by 254 nm UV lamp and the heating rate was kept constant in each cycle.

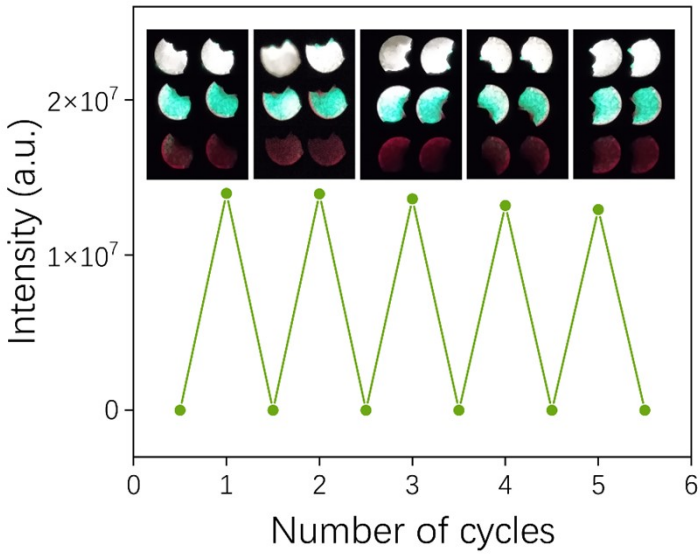

Figure S36. Thermal repeatability of the $SrGa_{12-x}Al_xO_{19}$: 4%Dy^{3+} (x=3) phosphor. TL-based temperature sensor was repeatedly checked via five cycle TL measurements. TL intensity was recorded as a function of number of cycles and the emission images were taken during the heating stage.

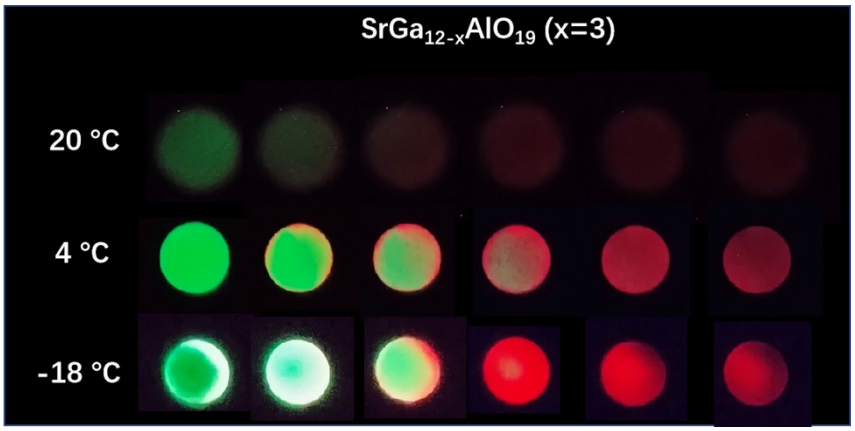

Figure S37. Photographs of $SrGa_{12-x}Al_xO_{19}$ (x=3) during thermally stimulated process. The sample was placed at varied ambient temperatures (at 20, 4, and –18 °C, respectively) for 64 h after excitation by 10-min 254 nm irradiation.

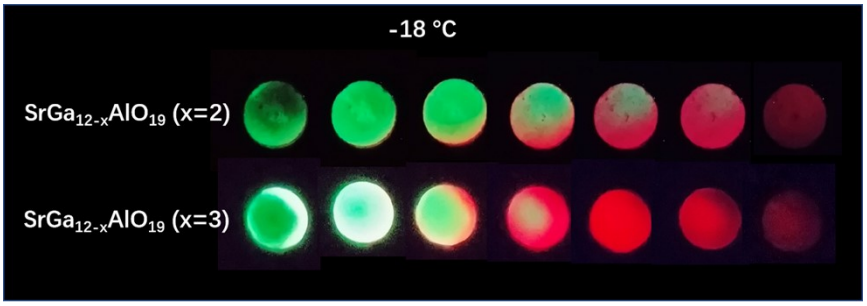

Figure S38. Comparison of $SrGa_{12-x}Al_xO_{19}$ (x=2) and $SrGa_{12-x}Al_xO_{19}$ (x=3) during thermally stimulated process. The samples were placed at –18 °C for 64 h after excitation by 10-min 254 nm irradiation.